Simulation and Dynamic Modeling of a Thermomechanical Ice Probe

Nathan L, Daniel *, E. Glenn Lightsey †
Georgia Institute of Technology, Atlanta, GA, 30332, USA

Ice-penetrating probes are useful tools for research on Earth, particularly for studying liquid water underneath or surrounded by ice. In recent decades, interest has grown in the use of ice probes for exploring the subsurface oceans thought to exist on some of the Solar System's icy worlds. While much work has been done on the thermal power requirements of such probes, little modeling work has been published on hybrid thermomechanical drilling probes. In this paper, a method is developed for simulating the descent trajectory of a hybrid thermomechanical probe through the ice shell of Jupiter's moon Europa. This method combines independent calculations of the velocity contributions from drilling and melting and a strategy for determining the conditions required for melting. Trajectories and descent time estimates are given for a range of different assumptions. Finally, the problem of melt probe attitude stability is briefly discussed and initial modeling efforts are presented.

I. Abbreviations

VERNE	=	Vertical Entry Robot for Navigating Europa
SESAME	=	Scientific Exploration Subsurface Access Mechanism for Europa
TRL	=	Technology Readiness Level
RTG	=	Radioisotope Thermal Generator
DNC	=	Did Not Converge
CFD	=	Computational Fluid Dynamics
LHR	=	Lateral Heating Requirement
FEA	=	Finite Element Analysis
NED	=	North-East-Down global frame
AP	=	Archimedes Principle

II. Nomenclature

T_{ice}	=	ambient ice temperature [K]
ρ_{ice}	=	density of ice [kg/m^3]
k_{ice}	=	thermal conductivity of ice [W/m-K]
$C_{p,ice}$	=	specific heat capacity of ice [J/kg-K]
α_{ice}	=	thermal diffusivity of ice [m^2/s]
T_{melt}	=	melting point of ice [K]
L	=	length of ice probe [m]
R	=	radius of ice probe [m]
A	=	cross sectional area of ice probe [m^2]
V	=	volume of ice probe [m^3]
m	=	mass of ice probe [kg]
ρ_{probe}	=	density of ice probe [kg/m^3]
I_{yy}	=	moment of inertia of ice probe [kg-m^2]
l_h	=	length of drill portion of ice probe [m]

*Graduate Student, Guggenheim School of Aerospace Engineering, 270 Ferst Drive, Atlanta, GA 30313, USA
†Professor, Guggenheim School of Aerospace Engineering, 270 Ferst Drive, Atlanta, GA 30313, USA

P_t = total available thermal power [W]
P_{elec} = total available electrical power [W]
ν_m = drilling motor efficiency
ν_g = drilling gearbox efficiency
E_{melt} = energy required to melt a volume of ice [J]
E_h = energy required to heat a volume of ice to the melting point [J]
E_L = energy required to complete phase change of a volume of ice already at the melting point
L_m = latent heat of fusion [J/kg]
L_m^* = reduced latent heat of fusion [J/kg]
$\vec{v}$ = velocity of probe [m/s]
$P_{h,ideal}$ = heat requirement at melt head without any efficiency corrections [W]
P_h = heat requirement at melt head [W]
γ = melt head efficiency correction
$P_{L,0}$ = lateral heat requirement to prevent melt pocket from refreezing
u = dummy variable of integration for calculation of lateral heat requirement
J_0 = zeroth order Bessel function of the first kind
Y_0 = zeroth order Bessel function of the second time
γ_{wat} = efficiency factor associated the thermal head power which contributes to the lateral heat requirement
γ_{ice} = efficiency factor associated with conduction of the heat in ice away from the probe head
$\vec{v}_{test}$ = ice probe velocity measured in field tests [m/s]
$\vec{v}_{sim}$ = simulated ice probe velocity [m/s]
$c_{\gamma,ice}$ = coefficient of power fit for γ_{ice}
$b_{\gamma,ice}$ = exponent of power fit for γ_{ice}
P_L = lateral heat requirement less the contribution of thermal head [W]
t_f = final time of ice penetration trajectory [yr]
P_{drill} = total mechanical power applied to ice by drill [W]
P_{shaft} = mechanical power output of drill gearbox [W]
$\vec{F}_{app}$ = contact force between the ice-probe and the ice directly below it [N]
P_{motor} = electrical power available for driving the drilling motor [W]
g = gravitational acceleration [m/s^2]
$\hat{z}_{ned}$ = downward unit vector
$\vec{F}_p$ = net fluid pressure force on the melt probe [N]
U = specific cutting energy of ice corresponding to drill design and operation [J/m^3]
γ_x = efficiency factor associated with the additionally energy required to transport ice chips
T_h = temperature of probe head; equivalently, temperature of ice in contact with drill (K)
$P_{h,required}$ = thermal power required to just initiate melting at melt head [W]
$P_{L,required}$ = thermal power required to just maintain a fluid film around the melt probe [W]
$P_{t,required}$ = total power required to just generate and sustain a melt pocket [W]
θ = pitch angle of ice probe [rad]
x_{CG} = center of gravity of ice probe [m]
x_{CB} = center of buoyancy of ice probe; equivalently, center of volume [m]
$B(\dot{theta})$ = hydrodynamic drag and damping buoyancy function
f_{CG} = ratio of ice probe center of mass to its length

III. Introduction

Jupiter's moon Europa is widely thought to have a deep, subsurface ocean lying beneath its icy shell. This ocean is a promising candidate for the search for extraterrestrial life; however, a probe capable of sampling the ocean and returning scientific data to earth would face challenges not encountered by any past space missions. The Vertical Entry Robot for Navigating Europa (VERNE) study was conducted at Georgia Institute of Technology in 2019-2021 as a response to the NASA Scientific Exploration Subsurface Access Mechanism for Europa (SESAME) call [1]. The purpose of the study was to design a spacecraft capable of penetrating Europa's ice shell in 3 years using technologies with a high Technology Readiness Level (TRL) in order to facilitate a launch date within the next 15 years. This design draws heavily on past work on ice-probes used on Earth on much smaller scales to explore subsurface water[2–6]. Ongoing tasks on the

project include TRL assessment and bench-top prototyping of some of the most promising low-TRL technologies.

The work described in this paper was done in order to support this study by developing a better understanding of the power required to achieve the 3-year target and informing design decisions and technology inclusions. The environmental model of Europa's ice shell and the design of the VERNE probe were both developed outside the scope of this paper, although they are described briefly in this section for reference. Due to the varying temperature throughout the ice shell and the potentially complex operations of VERNE's thermomechanical drill, the problem of estimating descent time was formulated as a 1-dimensional trajectory simulation rather than, for example, a simple calculation of the average descent rate. Initial efforts to extend this simulation into 2-dimensions, e.g. by assessment of melt probe pitch stability, are described as well.

A. Europa's Ice Shell Properties

As directed in the SESAME call, a total ice shell thickness of 15 km was assumed, which sits between the low estimate of just a few kilometers and the upper estimate of 30 km [7, 8]. The model of Europa's ice shell used in this paper accounts for two separate regions of ice, as are commonly theorized to exist [9, 10]. The upper region is comprised of cold, brittle ice where heat transfer occurs mainly through conduction, creating a temperature gradient from the surface temperature (110 K at the equator) to a basal temperature (260 K). The lower region, assumed here to begin at 5 km depth, is comprised of warmer, ductile ice where heat may be transferred through solid state convection. This convective ice layer is relatively isothermal and likely temperate (i.e. close to the melting point of ice). The most abundant salt in Europa's shell is thought to be either $MgSO_4$ or $NaCl$, although other salts have also been observed. [11, 12]. Even the small quantities quantities present are enough to change the melting temperature, density, and thermal diffusivity of the shallowest ice layers.

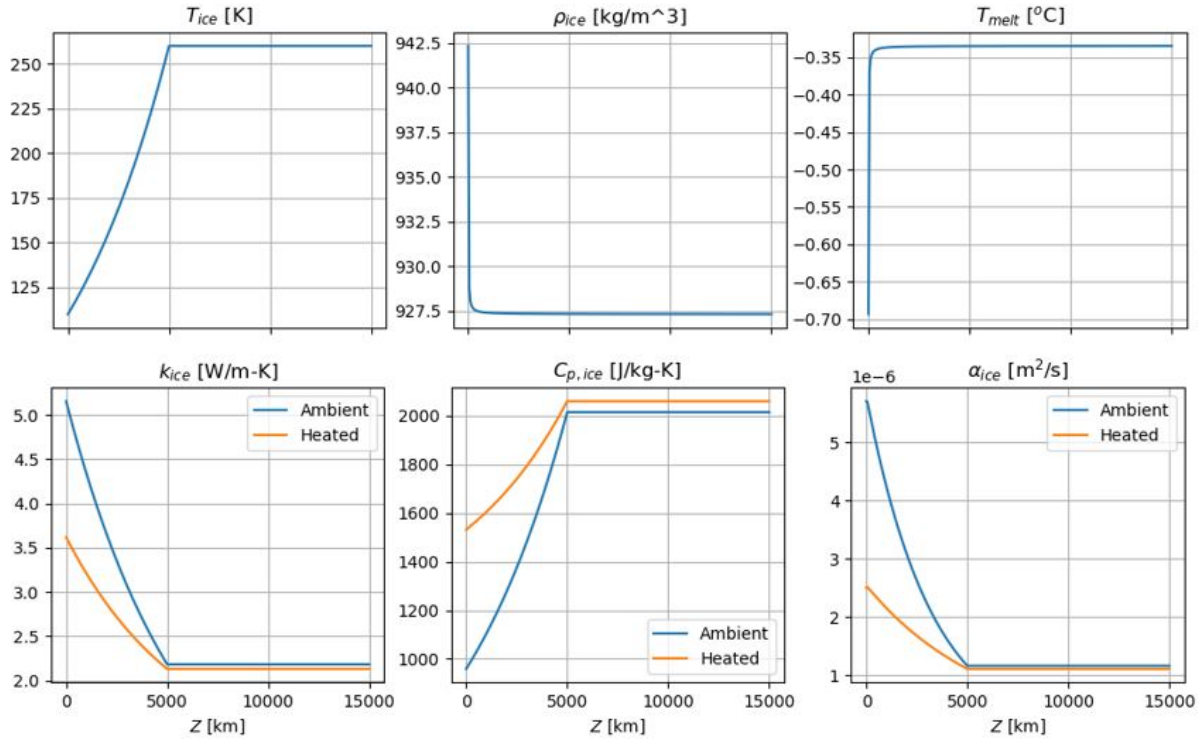

Fig. 1 Properties of europan ice shell vs depth, given the assumptions (conductive depth = 5 km; total depth = 15 km; surface temperature = 110 K; basal temperature = 260 K; most common salt = $MgSO_4$). For temperature dependent properties, both the ambient values and the average values during heating to the melting point are shown.

These assumptions allow the plotting of several key ice parameters shown in Figure 1 including ice temperature,

density, thermal conductivity, specific heat capacity, thermal diffusivity, and melting temperature (T_{ice}, ρ_{ice}, k_{ice}, $C_{p,ice}$, α_{ice}, T_{melt}). The orange lines shown in some of the plots give the temperature-dependent properties at the average of T_{melt} and T_{ice}. Using these values in the equations that represent the ice being heated from T_{ice} to T_{melt} gives higher fidelity results without much added complexity.

B. VERNE Probe

VERNE is a hybrid thermo-mechanical probe; that is, it uses both thermal melting and mechanical drilling to penetrate the ice. It is powered by three Radioisotope Thermoelectric Generators (RTGs), providing 300 W of electrical power (of which 160 W are available for drilling) and 6000 W of raw thermal power, which may be distributed to the probe head or side wall heaters by means of a pumped fluid loop. The head of the probe is a 2-part, counter-rotating cone with auger-like teeth. Further relevant properties are given in Table 1 and a complete description may be found in [1].

Table 1 Properties of the VERNE Probe [1]

Quantity	Symbol	Value	Units
Length	L	4.75	m
Radius	R	0.175	m
Cross-sectional Area	A	0.0962	m^2
Volume	V	0.457	m^3
Mass	m	480	kg
Density	ρ_{probe}	1050	kg/m^3
Moment of Inertia About Tip	I_{yy}	740	$kg\text{-}m^2$
Drill Length	l_h	0.25	m
Available Thermal Power	P_t	6000	W
Available Electrical Power	P_{elec}	160	W
Motor Efficiency	ν_m	0.83	–
Gearbox Efficiency	ν_g	0.86	–

IV. Hybrid Trajectory Dynamics

A. Overview of Hybrid Drilling

There are advantages in the use of a mechanical ice drill specific to the application of exploring Europa's ice shell. Initial penetration of the ice will occur in near vacuum, meaning that extra thermal power must be input to the highly conductive, cryogenic ice in order to sublimate it [13–15]. It is not clear how long it would take for enough pressure or condensation to build up to allow melting to take place; however, testing in [13] indicates the initial penetration could be characterized by intermittent sublimation, melting, and freezing in, adding undesirable risk to a critical portion of the trajectory. In addition, there is a high probability of encountering layers of salty or dusty ice which could be difficult or impossible to melt through [16]. Relying on mechanical drilling in these scenarios is one possible solution to both problems.

From the perspective of available power, however, it is highly beneficial to include thermal melting. For such a long duration mission travelling such a great distance, neither batteries nor copper power cables are feasible primary power options. Radioisotope heat sources are frequently used to provide electrical power to spacecraft in remote environments, and compact nuclear reactors have been proposed as a future solution [17, 18]. These technologies provide much more waste heat than electrical power [17], and an ice-penetrating probe is one scenario in which this waste heat can be readily put to use.

Hybrid ice drilling combines the advantages of thermal and mechanical drilling and reduces their respective disadvantages at the cost of being more difficult to design and model. As stated, mechanical drills can penetrate media that a melting probe could not, and even in pure ice mechanical drilling is more efficient than thermal drilling (i.e. a

higher descent rate is achievable with the same power [18, 19]). However, mechanical ice drills often face problems transporting the chipped ice from their front to their back, a problem that is eliminated when the ice is simply melted. If a combination of melting and drilling is used, the probe instead generates an ice-water mixture or slush which can be made to flow past the probe through careful design of the drill head [18, 20].

The mathematical relationship between thermal power and descent velocity of a pure melt probe is a well-explored problem (see [3, 21**?** –26] for sampling of literature). Computational fluid dynamics (CFD) analyses have been performed on a hybrid melt and hot water jet probe [27]. However, while hybrid thermomechanical drills have been tested and are in development [18, 20], no work has yet been published on mathematical modeling of their trajectories. The goal of the modeling described in this section is to address several questions on the application of a hybrid thermomechanical probe for reaching the sub-surface ocean on Europa, including

- When is a melt pocket generated and sustained?
- How much power is required to meet a given mission requirement?
- How should thermal power be distributed around the melt probe?

B. Thermal Modeling

1. Melting Power

The energy required to melt a given volume of ice is the sum of the energy required to raise its temperature to the melting point and the additional energy required to complete the phase change of that volume of ice. Mathematically,

$$E_{melt} = E_h + E_L = \rho_{ice} V C_{p,ice} (T_{melt} - T_{ice}) + \rho_{ice} V L_m \tag{1}$$

where L_m is the latent heat of fusion of ice. This expression is often simplified by defining the reduced latent heat of fusion, L_m^*, such that

$$E_{melt} = \rho_{ice} L_m^* V \tag{2}$$

In order to achieve a velocity $|\vec{v}|$ through ice, a melt probe must a achieve a volumetric melt rate of

$$\frac{dV}{dt} = A|\vec{v}| \tag{3}$$

where A is the cross-sectional area of the probe in the direction of travel. Then the power required at the thermal probe's melt head to achieve this velocity is

$$P_{h,ideal} = \frac{dE_{melt}}{dt} = \rho_{ice} L_m^* \frac{dV}{dt} = \rho_{ice} L_m^* A|\vec{v}| \tag{4}$$

Practically, not all of this power can be used directly for melting; sources of external loss include excess heating and convection in the melt pocket and conduction of heat through the ice away from the phase change boundary. This inefficiency can be modeled as

$$P_h = \frac{P_{h,ideal}}{\gamma} = \frac{\rho_{ice} L_m^* A|\vec{v}|}{\gamma} \tag{5}$$

where $\gamma \leq 1$. Parameters similar to γ have been estimated analytically [25] and experimentally [15, 21, 26], with estimates varying widely (0.6 – 0.95) based on ice conditions and melt head design. Thus, eq. (5) provides the absolute minimum thermal power requirement. Using it to simulate the descent of the VERNE probe with $\gamma = 1$ results in the trajectory shown in Fig. 2, which indicates that it would take no less than 2.88 years for the VERNE probe to descend through a 15 km Europa ice shell using only melting. However, as will be seen in the following section this is quite a large underestimate.

2. Lateral Heating Requirement

A large amount of thermal power is also required to prevent the melt pocket from refreezing around the probe. This power is referred to as the Lateral Heating Requirement (LHR) and is calculated by solving the problem of heat

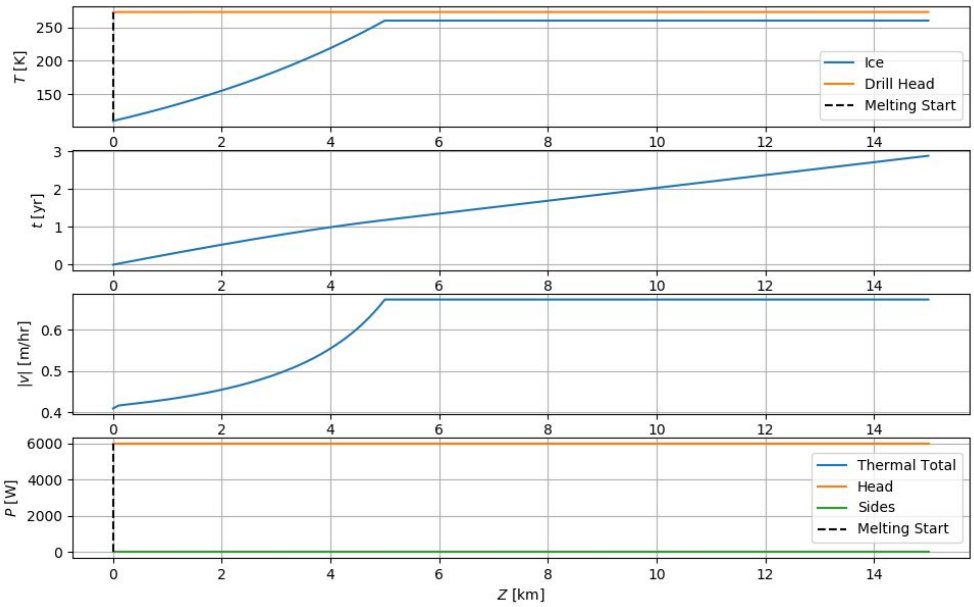

Fig. 2 Simulation of VERNE probe descent trajectory, accounting only for melt power; from top to bottom, temperature vs depth, time vs depth, descent velocity vs depth, and thermal power vs depth.

conducted away from a cylinder of fixed temperature (in this case, T_{melt}). This solution was presented in an earlier edition of [28] – and is referenced in [3, 25] – as

$$P_{L,0} = \frac{4k_{ice}(T_{melt} - T_{ice})}{R\pi^2} \int_0^L \int_0^\infty \frac{e^{-\alpha_{ice}u^2 \frac{l}{|\vec{v}|}}}{u(J_0^2(Ru) + Y_0^2(Ru))} dudl \tag{6}$$

where L is the length of the probe and R is its radius, J_0 and Y_0 are Bessel functions of the first and second kind, and u is a dummy variable of integration.

Formulations presented in [3, 25, 26] each assume that this power is partially provided by the melt head (through creation of an oversized borehole or excess heating of the melt water pocket) and partially – if necessary – by side wall heaters along the probe's lateral surface. To incorporate this effect into a model of a melt probe, the aforementioned efficiency factor γ is broken up into γ_{wat} – which represents the energy from the thermal head which contributes to the LHR – and γ_{ice} – which represents the unusable lost energy conducted away through the ice. The thermal power that must be applied at the probe head is then

$$P_h = \frac{P_{h,ideal}}{\gamma_{wat}\gamma_{ice}} = \frac{\rho_{ice}L_m^* A|\vec{v}|}{\gamma_{wat}\gamma_{ice}} \tag{7}$$

and the power that must be applied by side wall heaters, i.e. the reduced LHR, is

$$P_L = P_{L,0} - (1 - \gamma_{wat})\frac{P_{h,ideal}}{\gamma_{wat}\gamma_{ice}} \tag{8}$$

Note that if $\gamma_{ice} = 1$, the total power requirement is

$$P_t = P_h + P_L = \frac{P_{h,ideal}}{\gamma_{wat}} + (P_{L,0} - (1 - \gamma_{wat})\frac{P_{h,ideal}}{\gamma_{wat}}) = P_{h,ideal} + P_{L,0} \tag{9}$$

which is independent of γ_{wat}, although the distribution of power between the head and side heaters is not.

The double integral required to calculate the LHR incurs a high computational cost in a simulation. An exponential fit to the formula has been used in several studies [22, 25] but was only fit to results that used the thermal properties (conductivity, diffusivity) of temperate ice (i.e. near the melting point) and can be shown to not accurately model the original integral at all temperatures and velocities (Fig. 3). The approach taken in this paper is to create an interpolation

grid with the axes shown in Table 2. The LHR integral was allowed to converge to within 1% at each value in the 22,500-point grid with a total run time of 25.2 hours (about 4 seconds per point; for comparison, each interpolated point takes less than 1 millisecond).

Table 2 Interpolation Grid Axes

Quantity	Symbol	Units	Min	Max	Spacing	Points
Probe radius	R	m	0.0345	0.388	Linear	10
Probe length	L	m	0.675	8.58	Linear	10
Descent velocity	$\|\vec{v}\|$	m/hr	0.0036	5.01	Logarithmic	15
Ice temperature	T_{ice}	K	100	260	Logarithmic	15

A set of 1000 random points was used to test a linear interpolation on this grid against the "true" integral value. The resulting mean percent error was very low (0.35%); however, the magnitude of the interpolation error skewed positive, which would result in an overestimation of the required power (equivalently, an underestimation of the achievable descent velocity). To correct this, a full-effect polynomial regression on the error was created. The R-axis was transformed to its logarithm, which reduced the initial high dependence of the error on R; the other axes remain in a linear scale. This result was then subtracted from the interpolated value to form an error-corrected interpolated value. A slightly worse spread in the percent error is accepted in exchange for improvements in other metrics, as is shown in Table 3. These critically include a zero mean error value and an error sign that appears mostly independent of the axis values (i.e. R, L, $|\vec{v}|$, T_{ice}), which is expected to result in more accurate simulations.

Table 3 Error Metric Improvement after Error-Correction of Interpolator

Metric	Before Correction	After Correction
μ Error (W)	53.8	0
μ % Error	0.347	-0.00705
σ Error (W)	298	190
σ % Error	1.79	1.99
Max Absolute % Error	10.2	9.14

3. Model Validation

Limited field test data of thermal probes is available. Of the data that is published, testing is often confined to laboratory testing of the thermal head only [26, 29] or does not provide information on the ice temperature [6, 22]. Data points found with sufficient information to validate the formulation presented here are shown in Table 4.

Table 4 Melt Probe Field Test Data

Probe Name	$R\ [cm]$	$L\ [m]$	$P_{t,max}\ [W]$	$P_{h,max}\ [W]$	$T_{ice}\ [K]$	$\|\vec{v}\|\ [m/hr]$	Reference
Philberth Century 2	4.6	2.5	3680	–	248.15	2.9	[2, 18]
EnEx-IceMole	9.55*	1.94	10880	2880	256.15	1.1	[6, 30]
Cryobot	6	1.25	418	–	263.15	0.434	[31]

*Probe has a square cross section; R selected for equivalent cross-sectional area.

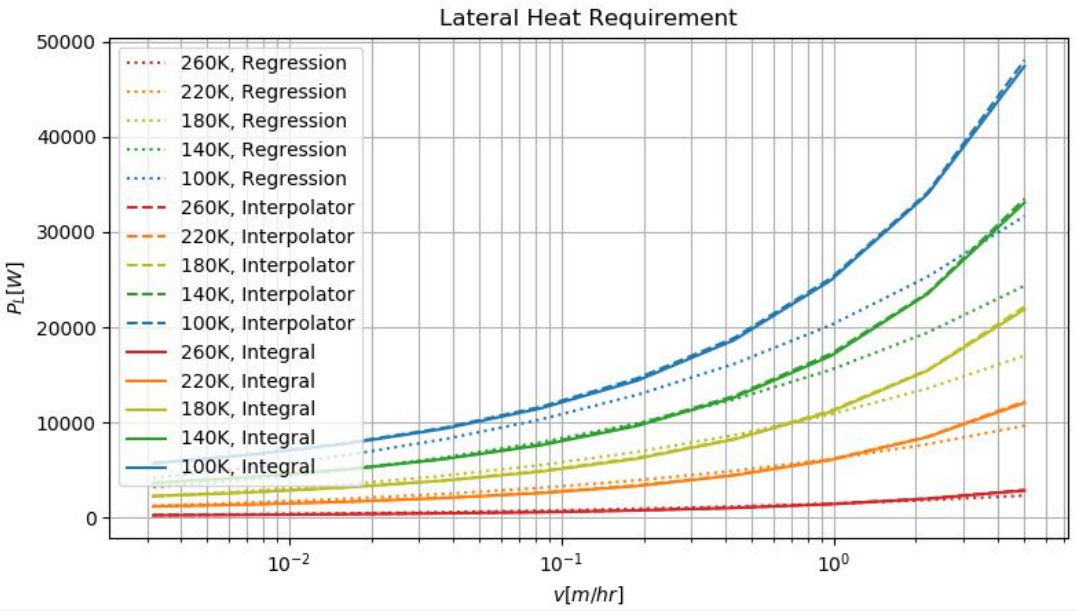

Fig. 3 Comparison of different LHR estimation techniques at varied ice temperatures and descent velocities. A close match is seen between the true integral and the grid interpolator, while the regression method gives inaccurate results at very low temperatures.

Using these probe properties, the descent rates were estimated from eq. (7) and eq. (8). The test benchmarks and the calculated values for $\gamma_{wat} = 0.6, 0.8, 1$, $\gamma_{ice} = 1$ are plotted in Fig. 4 against the temperature change required to initiate melting ($T_{melt} - T_{ice}$).

The model equations clearly provide representative estimates, but the percent error between the calculations and benchmarks is quite large (30% - 50%) and there is a predictable dependence on the ambient ice temperature. This discrepancy with field test data is used to find a power regression for γ_{ice} of the form

$$\gamma_{ice} = \frac{|\vec{v}_{test}|}{|\vec{v}_{sim}|} = c_{\gamma,ice}(T_{melt} - T_{ice})^{b_{\gamma,ice}} \tag{10}$$

where $c_{\gamma,ice}$ and $b_{\gamma,ice}$ are the curve fit parameters of the power regression. The full equations for calculating the required thermal power and which are used for trajectory simulations in this paper then become

$$P_h = \frac{\rho_{ice} L_m^* A|\vec{v}|}{\gamma_{wat} c_{\gamma,ice}(T_{melt} - T_{ice})^{(b_{\gamma,ice})}} \tag{11}$$

$$P_L = \frac{4k_{ice}(T_{melt} - T_{ice})}{R\pi^2} \int_0^L \int_0^\infty \frac{e^{-\alpha_{ice} u^2 \frac{l}{|\vec{v}|}}}{u(J_0^2(Ru) + Y_0^2(Ru))} du dl - (1 - \gamma_{wat}) P_h \tag{12}$$

Selecting $\gamma_{wat} = 0.8$ (a value roughly in the center of the range of estimates and which provides the lowest average percent error in Fig. 4), the values of the regression coefficients are determined and the resulting velocity estimates are plotted in Fig. 5. It should be noted that these values for γ_{wat}, $c_{\gamma,ice}$, and $b_{\gamma,ice}$ were generated from only these few test points, which are additionally all at relatively high ice temperatures compared to those which occur on Europa. Further testing data – especially at lower temperatures – would allow higher fidelity values to be recalculated.

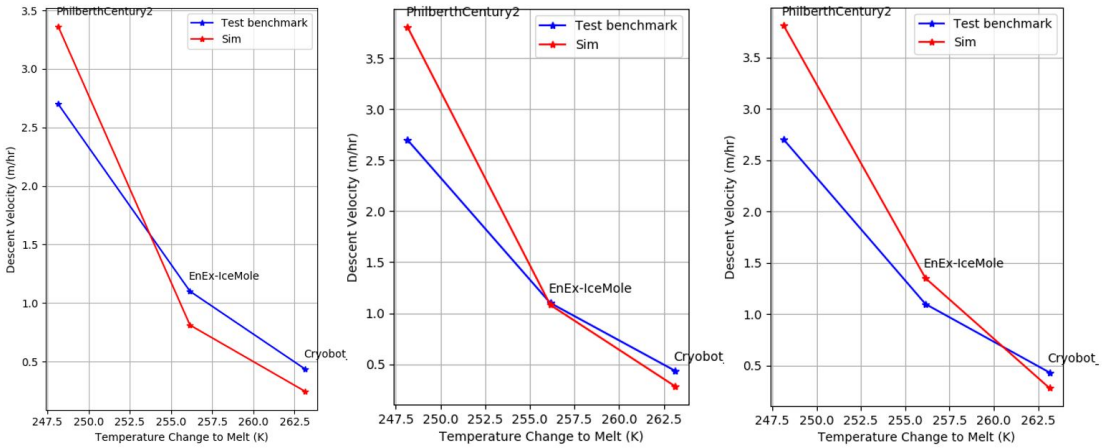

Fig. 4 Simulated descent rates and Test benchmarks vs Temperature change to melt; from left to right, γ_{wat} = 1 (avg. error = -15%), γ_{wat} = 0.8 (avg. error = +1.4%), γ_{wat} = 0.6 (avg. error = +9.6%)

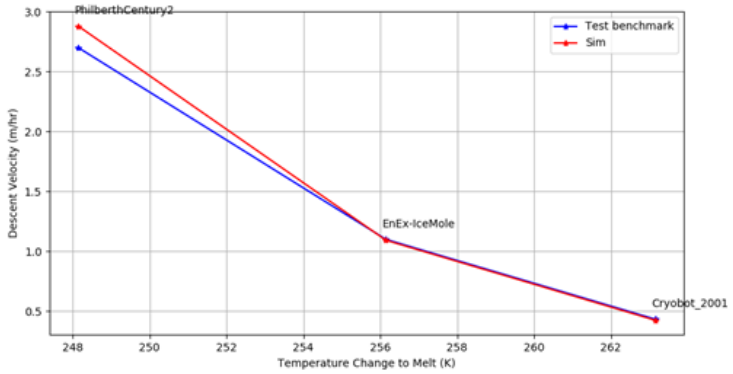

Fig. 5 Simulated descent rates and Test benchmarks vs Temperature change to melt; γ_{wat} = 0.8, $c_{\gamma,ice}$ = 10.745383, $b_{\gamma,ice}$ = −0.866852

4. Thermal Descent Simulation

When designing a melt probe, it is useful to obtain the power requirement as a function of the desired descent rate; however, when simulating the trajectory of a known melt probe the inverse relationship must be solved for. Since there is some difficulty in solving eq. (12) explicitly for $|\vec{v}|$, an iterative approach is taken. Given a total available thermal power of P_t, an initial estimate for the descent velocity, $|\vec{v}|_0$ is provided. Then, the following procedure is iterated on:

1) $P_{L,k}$ (e.g. $P_{L,1}$) is calculated from eq. (12) or a grid interpolator using $|\vec{v}|_{k-1}$ (e.g.$|\vec{v}|_0$)
2) $P_{h,k}$ (e.g. $P_{h,1}$) is calculated as the power remaining after subtracting $P_{L,k}$ (e.g. $P_{L,1}$) from P_t
3) $|\vec{v}|_k$ (e.g. $|\vec{v}|_1$) is calculated according to eq. (11).

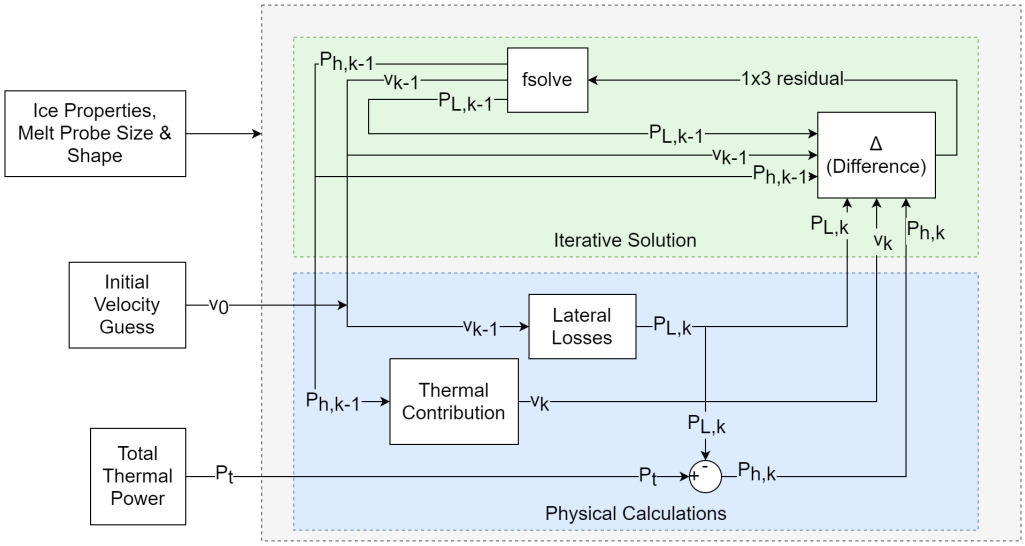

Fig. 6 Melting descent rate solution algorithm

The solver iterates until P_h, P_L, and $|\vec{v}|$ have converged. A diagram of this procedure is shown in Fig. 6. No guarantee of unique convergence is yet provided; however, it typically converges in less than 100 iterations even from non-ideal initial points (e.g. to a very low $|\vec{v}|$ despite a high initial guess).

The error-corrected interpolator with all efficiency corrections described in the previous section runs in 4.0 sec on a typical laptop computer and generates the trajectory shown in Fig. 7 with a descent time of 32.3 years – more than 10x the descent time when LHR is not accounted for. In the lowest plot, the distribution of power between the thermal head and side heaters is shown, and it may be noted that below an ice temperature of about 200K the majority of the thermal power must be used to satisfy LHR. This results in a much slower descent rate throughout the conductive ice shell layer and is responsible for the much higher overall descent time observed. Simulation run times and descent times for several other calculation techniques and efficiency corrections are shown in Table 5 for comparison.

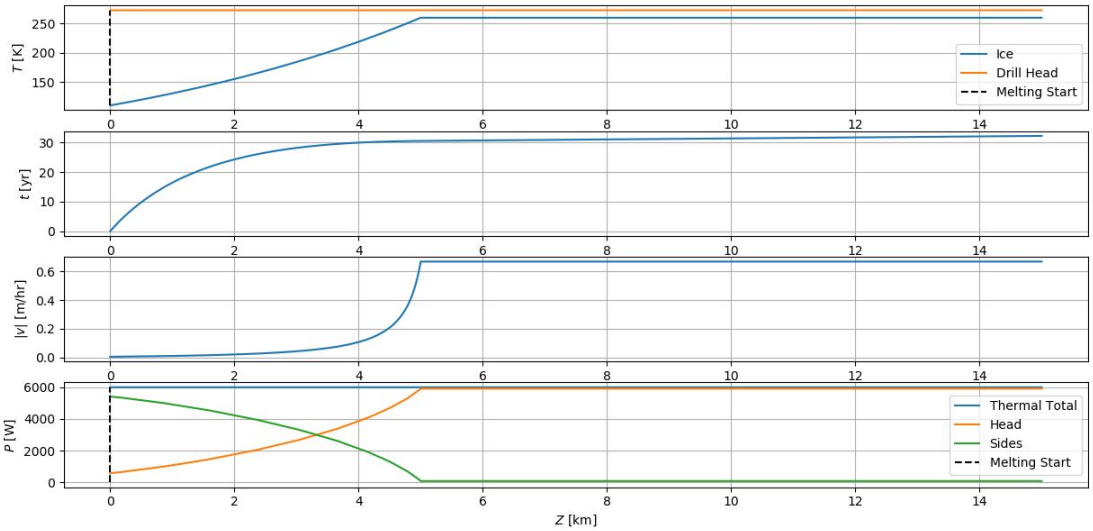

Fig. 7 Thermal Descent Trajectory after accounting for LHR

Table 5 Thermal Melting Descent Times

LHR Technique	γ_{wat}	$c_{\gamma,ice}$	$b_{\gamma,ice}$	Run Time (s)	t_f [yr], step=100m	t_f [yr], step=10m
Regression	1	1	0	0.22	17.6	17.6
Interpolator	1	1	0	4.5	20.6	20.2
Integrator	1	10.745383	-0.866852	721	34.5	33.8
Regression	1	10.745383	-0.866852	0.22	29.8	29.8
Interpolator	1	10.745383	-0.866852	3.8	34.3	34.3
Integrator	0.8	10.779223	-0.841258	1151	31.7	31.8
Regression	0.8	10.779223	-0.841258	0.31	28.1	28.1
Interpolator*	0.8*	10.779223*	-0.841258*	4.0*	32.3*	32.3
Integrator	0.6	13.275423	-0.849149	1344	29.6	29.7
Regression	0.6	13.275423	-0.849149	0.29	26.2	26.1
Interpolator	0.6	13.275423	-0.849149	4.1	31.1	30.3

*Trajectory shown in Fig. 7.

C. Mechanical Modeling

The power applied by a mechanical drill to the ice is the sum of the rotational mechanical power and the rate of work done by the applied force

$$P_{drill} = P_{shaft} + \vec{F}_{app} \cdot \vec{v} = \nu_m \nu_g P_{motor} + (mg\hat{z}_{ned} + \vec{F}_p) \cdot \vec{v} \tag{13}$$

where ν_m and ν_g are the efficiencies of the motor and gearbox, respectively, P_{motor} is the electrical power applied to drill motor, $mg\hat{z}_{ned}$ is the weight of the probe, and $\vec{F}_p$ is the fluid pressure force felt by the probe. Due to the low gravitational acceleration on Europa and very low descent velocity, the second term is very small compared to the first. Consequently, no significant error should arise from letting $\vec{F}_p$ be the buoyant force according to Archimedes' Principle (AP) ($\vec{F}_p = -\rho_{wat} g V \hat{z}_{ned}$). In general, however, this is not assumed to be the case for a melt probe, as is discussed in Section V.

In mechanical drilling, the specific cutting energy U of a medium plays an identical roll to the quantity $\rho_{ice} L_m^*$ in melting equations; that is, it gives the amount of energy required to chip through one cubic meter of ice [32, 33]. This result in

$$\frac{UA|\vec{v}_m|}{\gamma_x} = P_{drill} = \nu_m \nu_g P_{motor} + (mg\hat{z}_{ned} + \vec{F}_p) \cdot \vec{v} \tag{14}$$

where $\gamma_x \leq 1$ is an efficiency factor that accounts for the additional energy required to transport chips from in front of the probe to behind it. While a velocity is present on both sides of eq. (14), it should be noted that the $\vec{v}$ that appears on the right hand is the total velocity of the probe while the $\vec{v}_m$ that appears on the left hand side represents only the rate that the probe's drill is able to chip the ice, or the mechanical contribution to the velocity. For a hybrid probe, these are not always equal.

The specific cutting can be modeled as depending primarily on the ice temperature (the ambient temperature T_{ice} in the unheated case), the drill speed ω, and the descent rate $|\vec{v}|$. Drill design parameters such as the torque and rake angle are partially accounted for in the pairing of P_{mech}, ω, and $|\vec{v}|$. Some limited experimental data is available on these relationships in [33], and this data was used to tune a full-effect polynomial regression which appears to be give an accurate sense of the trend and slope over the data set (Fig. 8).

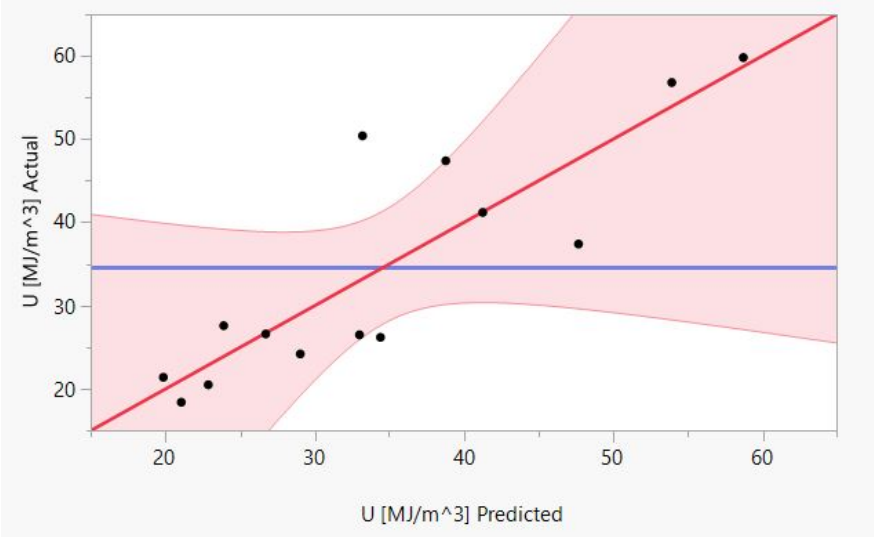

Fig. 8 Actual mechanical cutting energy vs Predicted mechanical cutting energy using full-effect polynomial regression.

A significant downside of this model is the level of extrapolation; while a value of ω was selected in the range of the data, the space explored by the descent rate solver and the values reached in the final trajectory stretch far outside the data set in the dimensions of temperature and descent velocity. This is shown in Fig. 9. In addition, the polynomial form of the regression allows it to become negative for some values of temperature and velocity. As a temporary solution to this problem, the simulation currently uses logistic functions to clamp U between 0.1 MJ/m^3 and 200 MJ/m^3 (a conservative range based on values of cutting energy given in [22]). However, the search for a cutting energy model that covers more of the relevant range remains part of ongoing work.

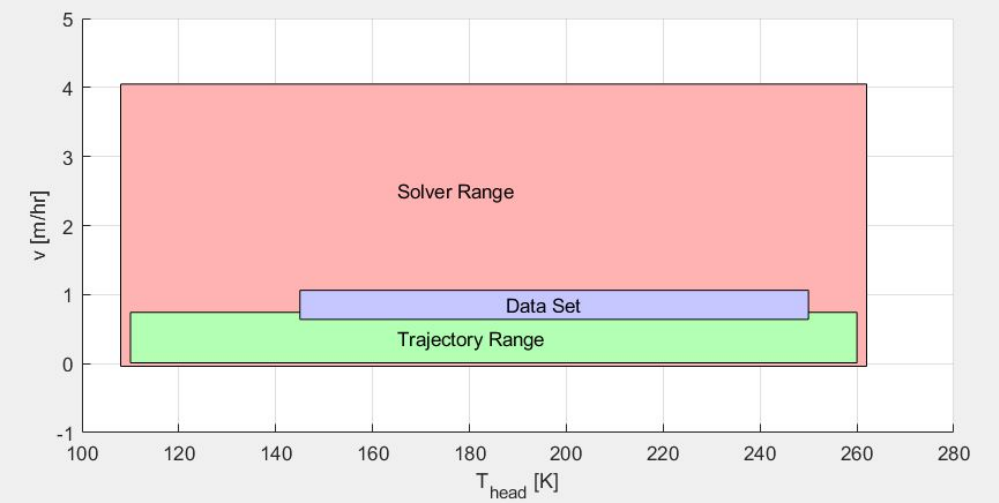

Fig. 9 Extrapolation visualization of mechanical cutting energy regression.

A simulated trajectory for a purely mechanical drill with $\gamma_x = 0.83$, $\nu_m = 0.83$, and $\nu_g = 0.86$ is shown in Fig. 10 with a descent time of 18.6 years; descent times under other assumptions are shown in Table 6. It should be noted that from about 4 km on, the cutting energy model is clipped to 0.1 MJ/m^3 as described above. This portion of the trajectory contributes a relatively small amount to the overall descent time due to the very high cutting energy of the cryogenic ice; however, the model is also extrapolating to temperatures outside of the data range at these points, and so the results should be taken with some caution. Descent times for different efficiency assumptions are given in Table 6.

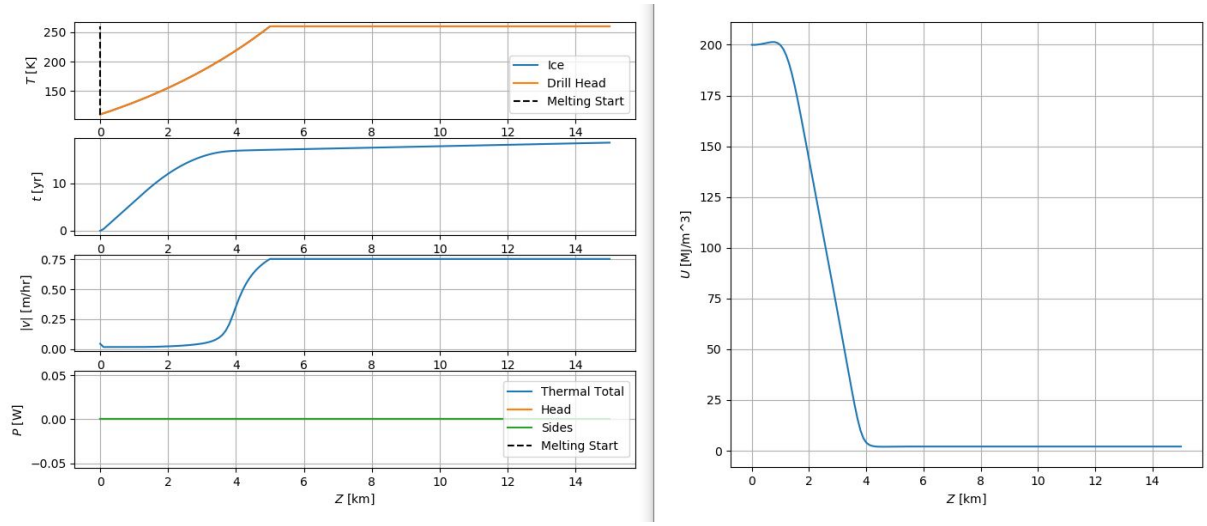

Fig. 10 Mechanical Drilling Trajectory; from left to right, trajectory quantities vs depth and cutting energy vs depth.

Table 6 Mechanical Drilling Descent Times

γ_x	ν_m	ν_g	t_f [yr], step=100m	t_f [yr], step=10m
1	1	1	11.6	11.4
1	0.83	0.86	15.7	15.4
1	0.67	0.72	22.8	22.4
0.83	1	1	13.7	13.5
0.83*	0.83*	0.86*	18.6*	18.3
0.83	0.67	0.72	26.8	26.3
0.67	1	1	16.6	16.4
0.67	0.83	0.86	22.7	22.3
0.67	0.67	0.72	32.8	32.3

*Trajectory shown in Fig. 10

D. Hybrid Modeling

Two additional results become relevant to the descent modeling at each point in a hybrid trajectory: the temperature of the drill head (equivalently, the temperature of the ice layer in contact with the drill head); and whether or not melting is allowed to take place.

1. Temperature of the Melt Head

The temperature of the probe drill head, T_h is approximately equal to the temperature of the ice being cut by the drill teeth. The higher this temperature, the lower the cutting energy U, and the higher the contribution of mechanical drilling to the descent velocity, $|\vec{v}_m|$. Therefore, even when no melting is occurring it is desirable to direct thermal power P_h to the probe head in order to increase T_h. In this "no-melting" case, the relationship between P_h and T_h is assumed to be similar in form to eq. (5), with the distinctions that the latent heat of enthalpy plays no role and that the melting temperature, T_{melt}, is replaced by T_h, where $T_h < T_{melt}$.

$$P_h = \frac{\rho_{ice} A |\vec{v}| C_{p,ice} (T_h - T_{ice})}{\gamma_{ice}} \Rightarrow T_h = T_{ice} + \frac{P_h \gamma_{ice}}{\rho_{ice} A |\vec{v}| C_{p,ice}} \tag{15}$$

Also note that the only inefficiency factor applied is γ_{ice}, representing the conduction of heat away from the ice directly in front of the probe. Since γ_{wat} only describes the widening of the melted borehole and the transfer of heat within the melt pocket, it plays no role if no melting is occurring.

Approaches to determining the head temperature of a probe during melting require either analysis of the flow and pressure characteristics of the melt film (e.g. through numerical simulation [24, 25, 34] or CFD tools [27]) or experimental data [26]). For example, the following closed form solution is presented in [25]:

$$T_h = T_{melt} + \frac{10(P_h^2 - \gamma^2 P_h^2}{C_{p,wat}\rho_{ice}A|\vec{v}|(3P_h + 7\gamma P_h)} \tag{16}$$

However, the body of the melt head and the phase boundary are thermally insulated by the melt film according to close contact melting assumptions [21, 24]; the phase boundary remains at the melting temperature T_{melt}. Since this is where the drill teeth actually contact the ice, the temperature relevant for calculating the cutting energy U is simply

$$\begin{cases} T_h = T_{ice} + \frac{P_h c_{\gamma,ice}(T_{melt} - T_{ice})^{b_{\gamma,ice}}}{\rho_{ice}A|\vec{v}|C_{p,ice}} & \text{if no melting occurs} \\ T_h = T_{melt} & \text{if melting occurs} \end{cases} \tag{17}$$

2. Conditions for Melting

Below a certain ice temperature, it may be possible to generate a melt pocket but not to sustain it given the available thermal power. This is a consequence of the very high thermal conductivity of cryogenic ice (Fig. 1), and the subsequent high LHR (eq. (6)). Identifying where in the ice shell this threshold occurs and disabling melting for the prior portion of the trajectory enables this high LHR to be ignored and more heat to be used for warming the drill. Several strategies for simulating when melting can or should take place have been tested, with results shown below.

The first option is to assume that melting always takes place. In the plot shown in Fig. 11, enough power to sustain a melt pocket is not actually available until past a depth of 4 km. However, because the simulation assumes that LHR still exists, the available thermal power is used for heating the sides of the probe rather than the drill head. In other words, thermal power is wasted trying to keep a nonexistent melt pocket from refreezing. Using this strategy results in a total descent time of about 12.7 years, which is less than either the pure melting case (Fig. 7) or the pure mechanical drilling case (Fig. 10).

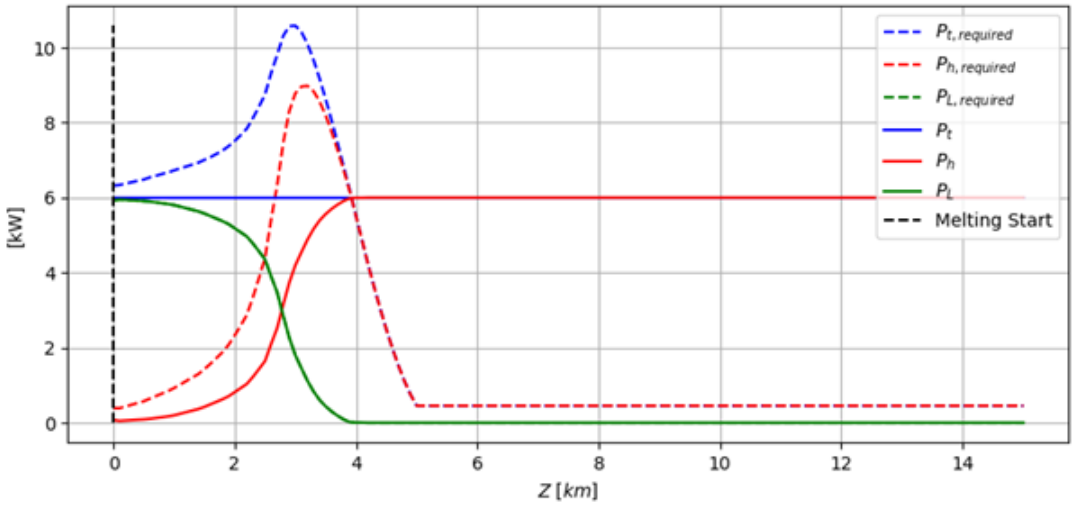

Fig. 11 Power and melting plot of hybrid trajectory; always melting. When a dotted and solid line of the same color intersect, it implies that there is just enough power raise the temperature of the ice to its melting point. The intersection P_t and $P_{t,required}$ gives the depth at which a stable melt pocket can be maintained.The area between P_h and $P_{h,required}$ gives some indication of the magnitude of the contribution of melting to the probe's descent velocity.

The second option is to assume melting takes place only when the melting temperature is reached ($T_h = T_{melt}$). Because there is no LHR prior to melting, $P_h = P_t$ and the lowest temperature at which this can occur is given by rearranging eq. (17) to arrive at

$$T_{ice} = T_{melt} + \frac{P_h \gamma_{ice}}{\rho_{ice} A |\vec{v}| C_{p,ice}} = T_{melt} + \frac{P_t \gamma_{ice}}{\rho_{ice} A |\vec{v}| C_{p,ice}} \tag{18}$$

This strategy makes intuitive sense, but practically it creates a convergence problem in the iterative solver. Upon reaching T_{melt}, the LHR instantly becomes nonzero, requiring an increase in P_L; this results in a decrease in the power available for heating the probe head, which causes T_h to fall back below T_{melt}, causing LHR to become 0 again and restarting the cycle. The physical meaning behind this is that allowing melting to occur as soon as it is achievable at the melt head will result in the probe repeatedly freezing itself into the ice and having to attempt to melt back out, which creates risk to the system the transition from no-melting to melting. In Fig. 12, the results of this are shown for several different simulation step sizes, with the inconsistency in descent time caused primarily by inconsistent convergence of the melt condition. Simulations using this condition are more accurate at larger step sizes which skip over more of the transition region.

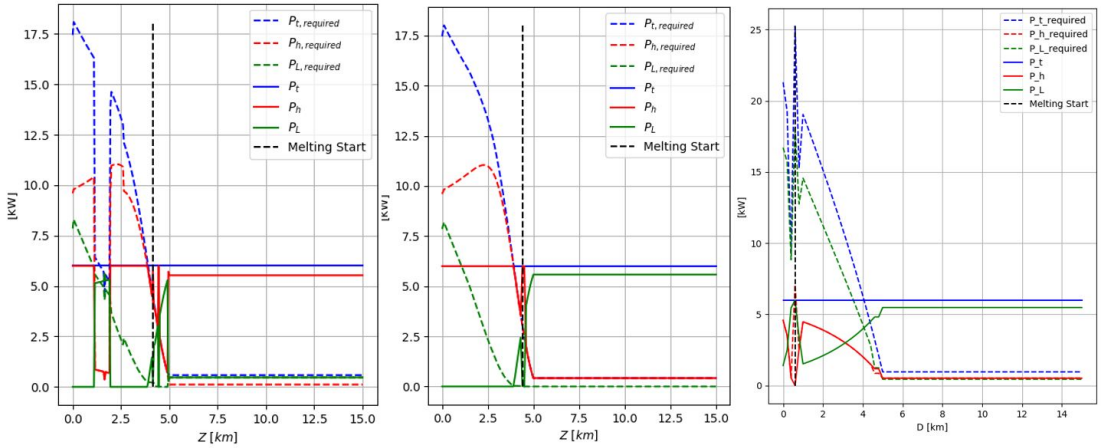

Fig. 12 Power and melting plot of hybrid trajectory; temperature melt condition. From left to right, step sizes of 50 m (4.4 years), 75 m (45.6 years), and 100 m (2.69 years).

The third and most consistent option is to allow melting only when there is enough power to sustain a stable melt pocket at the given velocity; in other words, when $P_t = P_{h,required} + P_{L,required}$, where the "required" subscript denotes a value calculated in a controlling computer or decision-making subroutine rather than a physical value. $P_{L,required}$ is identical to the value returned by either the LHR integral or grid interpolator, while $P_{h,required}$ is the power required to initiate melting as given in eq. (18). This method results in a continuous transition between pure mechanical drilling and hybrid drilling, as can be seen in Fig. 13, and a lower descent time than any of the other methods at 2.06 years.

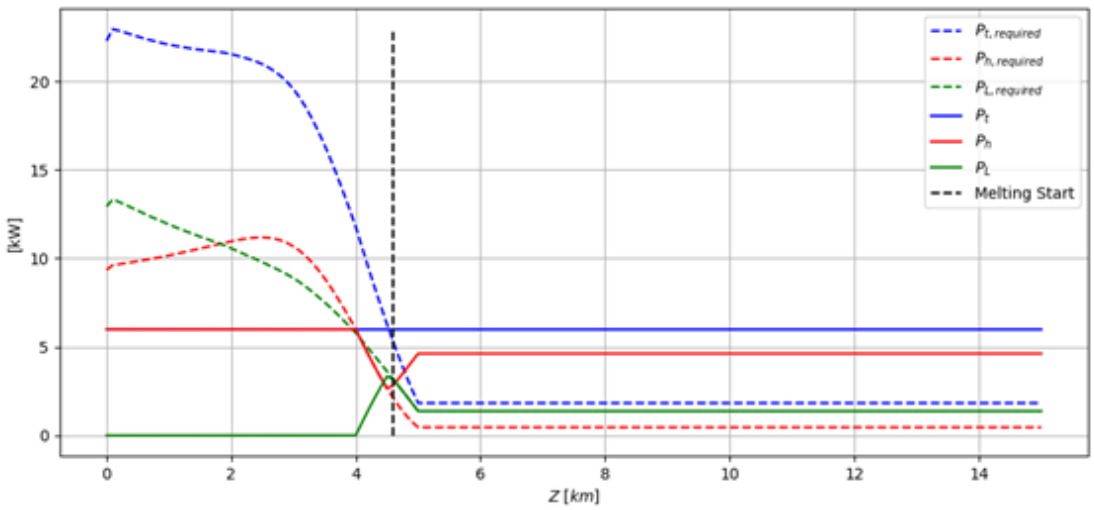

Fig. 13 Power and melting plot of hybrid trajectory; power melt condition.

A fourth and final strategy is to consider that no melting takes place. Benefits are still achieved from the thermal power because heating the ice lowers its cutting energy and makes the mechanical drilling more efficient; additionally, this assumption means that no thermal power is required to keep a melt pocket open for the entire descent. The significant downsides are that no additional ice chip transport assistance is provided and no melt water is generated which may be sampled by probe science instruments.

3. Hybrid Descent Simulation

The iterative procedure shown in Fig. 6 may be altered to account for the additional mechanical contribution to the descent velocity. Because of the complexities of thermomechanical drilling and melting, it is not fully understood how the two are combined, and intuition does not always hold. From the perspective of energy imparted to the ice, one might think they are additive. However testing data from [20], which used a similar drill design to VERNE, indicates that the actual velocity achieved by a thermomechanical drill may be only the minimum of the mechanical and thermal contributions; that is, the velocity "contributions" are constraining. Although practically it may be a combination of these scenarios, three cases are demonstrated in this paper: minimum (a.k.a. constraining), maximum (a.k.a. enabling), and additive.

As before, a total available thermal power P_t and an initial estimate for the descent velocity $|\vec{v}|_0$ are provided. In addition, the electrical power used to drive the drill, P_{elec}, is given. Then, the following procedure is iterated on:

1) $P_{L,required,k}$ is calculated from eq. (12) or a grid interpolator using $|\vec{v}|_{k-1}$.
2) $P_{h,required,k}$ is calculated from eq. (11).
3) If $P_t > P_{h,required,k} + P_{L,required,k}$, melting occurs and $P_{L,k} = P_{L,required,k}$, $P_{h,k} = P_t - P_{L,k}$, and $|\vec{v}|_{t,k}$ is calculated from $eq.$ (11).
4) $|\vec{v}|_{m,k}$ is calculated from eq. (14), using U corresponding to $|\vec{v}|_{k-1}$ and $T_{h,k-1}$.
5) $|\vec{v}|_k$ is calculated based on the assumption:
    1) Minimum/Constraining: $|\vec{v}|_k = min\{|\vec{v}|_{t,k} \setminus 0, |\vec{v}|_{m,k} \setminus 0\}$ (where $\setminus 0$ indicates that a velocity of 0 is not accepted unless both are 0).
    2) Maximum/Enabling: $|\vec{v}|_k = max\{|\vec{v}|_{t,k}, |\vec{v}|_{m,k}\}$
    3) Additive: $|\vec{v}|_k = |\vec{v}|_{t,k} + |\vec{v}|_{m,k}$
6) $T_{h,k}$ is calculated using eq. (17) and $|\vec{v}|_k$.

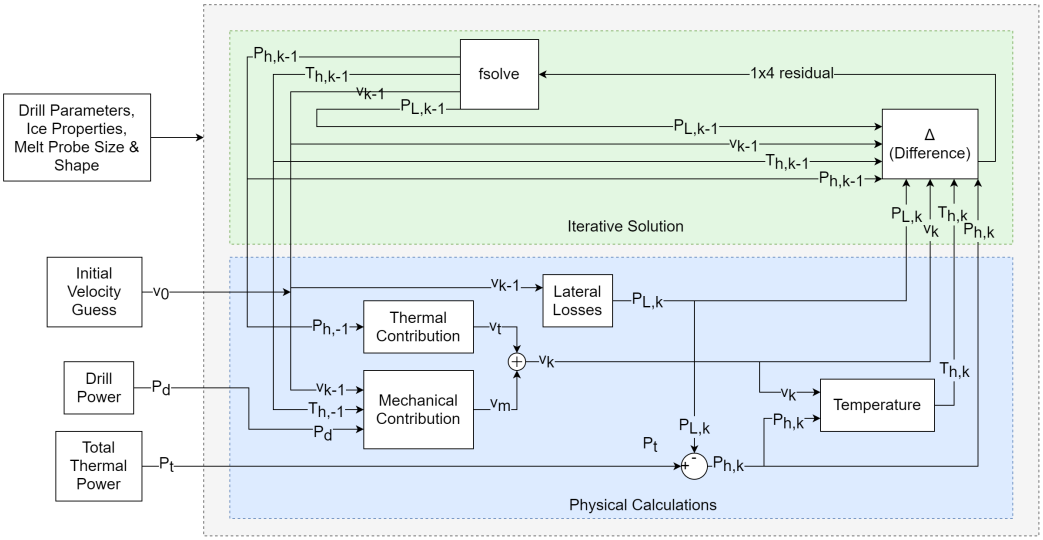

Fig. 14 Hybrid descent rate solution algorithm

The solver iterates until the melt power P_h, lateral power P_L, descent velocity $|\vec{v}|$, and melt head temperature T_h have all converged. A diagram showing this procedure is given in Fig. 14. Again, no guarantee of unique convergence is yet derived for this solution procedure. Due in part to complications from incorporating the mechanical model, successful convergence appears to be highly dependent on the residual weights and initial guess.

Simulated trajectories generated with this technique are shown in Fig. 15 using each assumption for combination of mechanical and thermal velocities – additive, minimum and maximum. By relying entirely on the warmed mechanical drill in the coldest ice, an order of magnitude higher descent rate is achieved than in the case of either a pure melt probe (Fig. 7) or mechanical drilling (Fig. 10), with each method resulting in a descent time of about 2 to 4 years. The corners in the power plots that occur after 4 km depth show the points at which melting starts; prior to this point, as much heat is applied to the drill head as is possible without generating any melt water while the side heaters are used merely to shed excess heat. A listing of descent times for a range of assumptions is given in Table 7, with failures to converge marked as Did Not Converge (DNC).

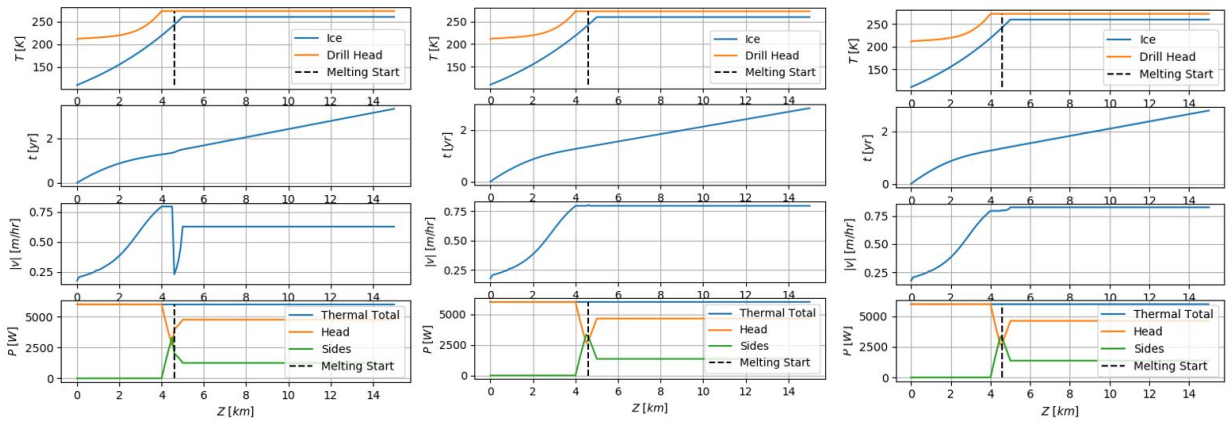

Fig. 15 Hybrid descent trajectories; power melt condition; from top to bottom, minimum, maximum, and additive velocity contributions.

Table 7 Hybrid Drilling Descent Times

Therm	LHR Method	γ_{wat}	$c_{\gamma,ice}$	$a_{\gamma,ice}$	Mech	γ_x	ν_m	ν_g	Melt Cond.	Contr. Method	t_f [yr] , step = 1000m	t_f [yr] , step = 100m	t_f [yr] , step = 10m
Yes	Regression	1	10.745383	-0.866852	–	–	–	–	Always	–	28.0	29.8	29.8
Yes	Interpolator	1	10.745383	-0.866852	–	–	–	–	Always	–	31.3	34.3	34.3
Yes	Regression	0.8	10.779223	-0.841258	–	–	–	–	Always	–	26.4	29.8	29.8
Yes	Interpolator	0.8	10.779223	-0.841258	–	–	–	–	Always	–	29.4	32.3	32.3
Yes	Regression	0.6	13.275423	-0.849149	–	–	–	–	Always	–	24.7	26.2	26.1
Yes	Interpolator	0.6	13.275423	-0.849149	–	–	–	–	Always	–	31.0	31.1	30.3
–	–	–	–	–	Yes	1	0.83	0.86	–	–	18.2	15.7	15.4
–	–	–	–	–	Yes	0.83	0.83	0.86	–	–	21.5	18.6	18.3
–	–	–	–	–	Yes	0.83	0.83	0.86	–	–	26.1	22.7	22.3
Yes	Regression	0.8	10.779223	-0.841258	Yes	0.83	0.83	0.86	Always	Min	DNC	DNC	DNC
Yes	Interpolator	0.8	10.779223	-0.841258	Yes	0.83	0.83	0.86	Always	Min	18.0	20.15	20.2
Yes	Regression	0.8	10.779223	-0.841258	Yes	0.83	0.83	0.86	Temp	Min	2.13	2.13	DNC
Yes	Interpolator	0.8	10.779223	-0.841258	Yes	0.83	0.83	0.86	Temp	Min	2.13	2.13	DNC
Yes	Regression	0.8	10.779223	-0.841258	Yes	0.83	0.83	0.86	Power	Min	3.13	3.11	3.12
Yes	Interpolator	0.8	10.779223	-0.841258	Yes	0.83	0.83	0.86	Power	Min	3.07	3.04	3.06
Yes	Regression	0.8	10.779223	-0.841258	Yes	0.83	0.83	0.86	Always	Max	DNC	DNC	DNC
Yes	Interpolator	0.8	10.779223	-0.841258	Yes	0.83	0.83	0.86	Always	Max	DNC	DNC	DNC
Yes	Regression	0.8	10.779223	-0.841258	Yes	0.83	0.83	0.86	Temp	Max	2.13	2.13	2.13
Yes	Interpolator	0.8	10.779223	-0.841258	Yes	0.83	0.83	0.86	Temp	Max	2.13	2.13	2.13
Yes	Regression	0.8	10.779223	-0.841258	Yes	0.83	0.83	0.86	Power	Max	2.13	2.13	2.13
Yes	Interpolator	0.8	10.779223	-0.841258	Yes	0.83	0.83	0.86	Power	Max	2.13	2.13	2.13
Yes	Regression	0.8	10.779223	-0.841258	Yes	0.83	0.83	0.86	Always	Add	DNC	DNC	12.5
Yes	Interpolator	0.8	10.779223	-0.841258	Yes	0.83	0.83	0.86	Always	Add	12.7	DNC	12.2
Yes	Regression	0.8	10.779223	-0.841258	Yes	0.83	0.83	0.86	Temp	Add	2.13	DNC	DNC
Yes	Interpolator	0.8	10.779223	-0.841258	Yes	0.83	0.83	0.86	Temp	Add	2.13	DNC	DNC
Yes	Regression	0.8	10.779223	-0.841258	Yes	0.83	0.83	0.86	Power	Add	2.06	2.06	2.06
Yes	Interpolator	0.8	10.779223	-0.841258	Yes	0.83	0.83	0.86	Power	Add	2.06	2.06	2.06
Yes	Any	Any	10.779223	-0.841258	Yes	0.83	0.83	0.86	Never	Any	2.13	2.13	2.13

V. Melt Probe Attitude Dynamics

Methods of controlling or stabilizing melt probes have been proposed in the past, and include ideas such as directed water jetting [19], a differentially heated melt head [34], a buoyant upper section [35], pendulum stabilization [36], and mercury steering [2]. Most of these techniques impose some additional mass, power, or complexity constraint on the probe [37], which in some cases might be quite drastic. For example, pendulum stabilization as described in [36] requires a secondary heater near the top of the probe (Labelled 24 in Fig. 16) with a larger diameter than the probe body (Labelled 21 in Fig. 16). This increases the required melt power proportionally to the square of the increase in diameter. Additionally, certain techniques may be incompatible with some probe designs; for example, differential heating is not compatible with the hybrid thermomechanical probe VERNE [1] since there is no known way to use it on a rotating melt head.

The justification for attitude stabilizing systems has typically been conjectural or experiential [4, 22, 35, 36] – rather than based on a physical model – or derived from another requirement such as the need for maneuverability [17–19, 30, 38]. It is indeed likely that over the course of a lengthy mission, a melt probe will encounter disturbing moments caused by voids in the ice, uneven melting, convection inside the melt pocket, and other unpredicted noise factors. However, no rigorous analysis has been performed on the passive stability of a vertical-oriented melt probe in response to this noise and in the absence of costly control techniques. This section describes some early steps taken toward development of this analysis.

A. Separation of Dynamic Regimes

The most critical dynamic behavior is the long-term shape of the melt probe's trajectory, which is driven by the dynamics of melting. From eq. (5), it's apparent that a higher cross-sectional area results in a lower descent rate. In addition, while the probe sides may be heated, the densest heat flux occurs at the tip of the probe. These properties imply that at least some probe designs are nonholonomic, which in this case means their achievable motion through ice is constrained by their orientation. An analogy may be drawn to the dynamics of a launch vehicle, in which the resistance to motion (drag) is also proportional to the cross-sectional area and the method of overcoming this resistance (thrust) is also directed along the vehicle longitudinal axis. As with a launch vehicle, the degree to which this constraint applies is expected to be dependent on key aspects of the probe design.

Several notional paths through the ice shell of an Ocean World such as Europa are given in Fig. 17, which it should be noted are not derived from a simulation but simply based on the interpretation of the melt probe as a dynamic system.

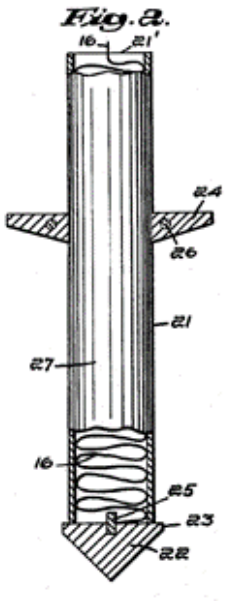

Fig. 16 Concept sketch for pendulum-stabilized thermal probe from Aamot 1968, Patent 3,390,729

Case 1 shows an ideal, undisturbed vertical trajectory which reaches the subsurface ocean in minimum time. Cases 2, 3, and 4 each show the effect of some disturbance which is persistent enough to affect the melt probe's trajectory. The response of a probe to this disturbance can be characterized as asymptotically stable if the probe returns to a vertical orientation (Case 2), Lyapunov stable if it remains within some minimum and maximum pitch values (Case 3), and unstable if it continues pitching until horizontal (Case 4). Of the cases which experience a disturbance, the asymptotically stable response achieves the minimum descent time, while the unstable case is likely to never reach the subsurface ocean.

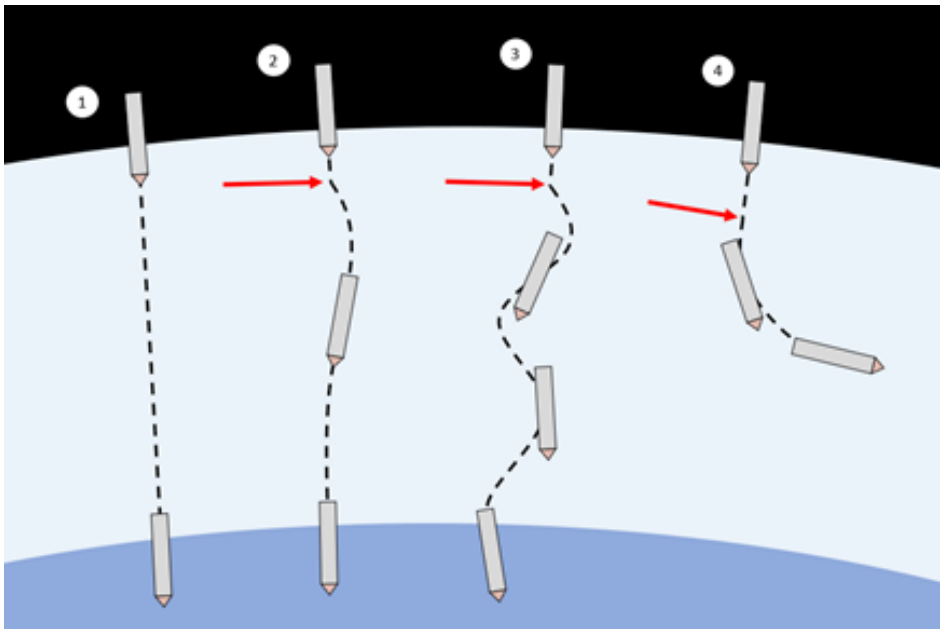

Fig. 17 Melting orientation dynamics; 1) Undisturbed, 2) Asymptotic, 3) Lyapunov, 4) Unstable

A separate dynamic regime also occurs within the melt pocket (see Fig. 18). The pressure forces exerted by the fluid in the melt pocket on the probe create their own dynamic behavior which may also be asymptotically stable (Case 1),

Lyapunov stable (Case 2), or unstable (Case 3).

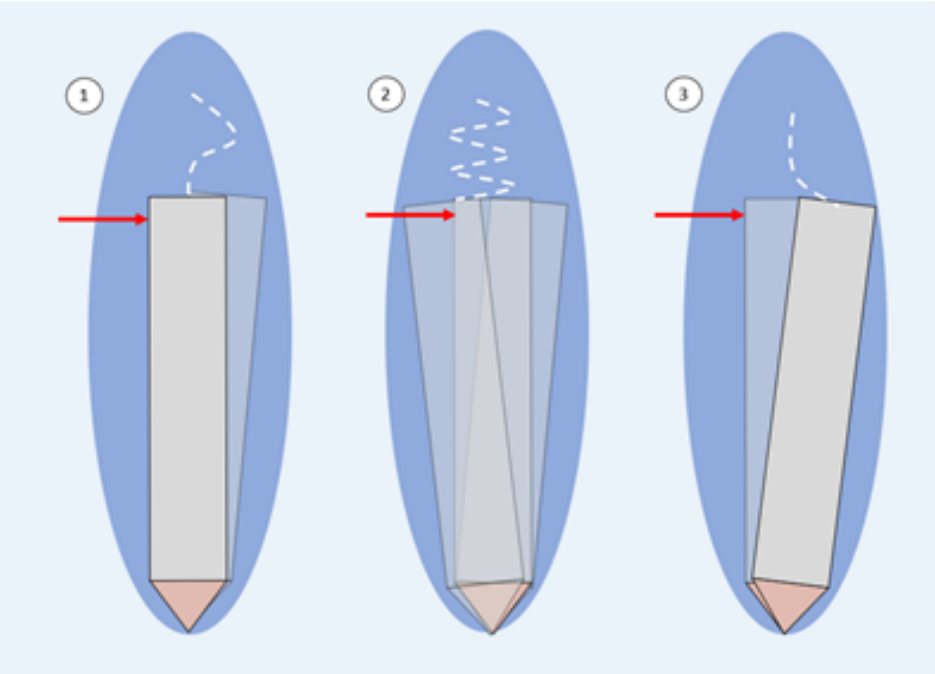

Fig. 18 Pressure dynamics within melt pocket; 1) Asymptotic, 2) Lyapunov, 3) Unstable. The shown melt pocket shape is only notional.

This separation of dynamics is thought to be valid due to the difference in time scales between the melting dynamics (driven by heat transfer) and the fluid dynamics (driven by the fluid flow). Framed another way, the resistance to motion through ice is much greater than the resistance to motion through water. This assumption could theoretically break down at a high enough melting power, but this is thought to be infeasible for a melt probe design (similar ideas are discussed in [25]). In the analysis of each regime, then, it may be assumed that only one system is dynamically relevant. Fig. 19 shows how this separation can notionally be used to analyze the probe's behavior (again, not yet based on simulation results or realistic physical properties) and to help illustrate the potential relationships between these regimes.

B. Static Buoyant Stability

The most intuitive way to examine the pressure dynamics is to consider the forces and moments on the melt probe due to its weight and its buoyancy. In [35] it is suggested that a melt probe can maintain a vertical attitude throughout its descent by adding a buoyant upper section to the probe. As is common in analyses of aquatic systems, [35] used Archimedes' Principle (AP) is used to express the pressure force:

$$\vec{F}_p = -\rho_{wat} g V \hat{z}_{ned} \tag{19}$$

where ρ_{wat} is the density of water and V is the volume of the melt probe. Assuming that the center of gravity x_{CG} and center of buoyancy x_{CB} both lie on the probe x-axis, the dynamic equation describing the rotation of the system is

$$\ddot{\theta} I_{yy} = mg|x_{CG}| \sin\theta - \rho_{wat} g V |x_{CB}| \sin\theta - B(\dot{\theta}) \tag{20}$$

Where m is the mass of the melt probe, I_{yy} is the moment of inertia about the probe y-axis (out of the page) at the tip of the melt head, θ is the pitch angle, and $B(\dot{\theta})$ is a function of the pitch rate which describes hydrodynamic drag and damping forces. This may be simplified and linearized using the small angle approximation, and by assuming that the damping forces are stabilizing and small in magnitude compared to the inertia of the probe:

$$\ddot{\theta} I_{yy} y = g(m|x_{CG}| - \rho_{wat} V |x_{CB}|)\theta \tag{21}$$

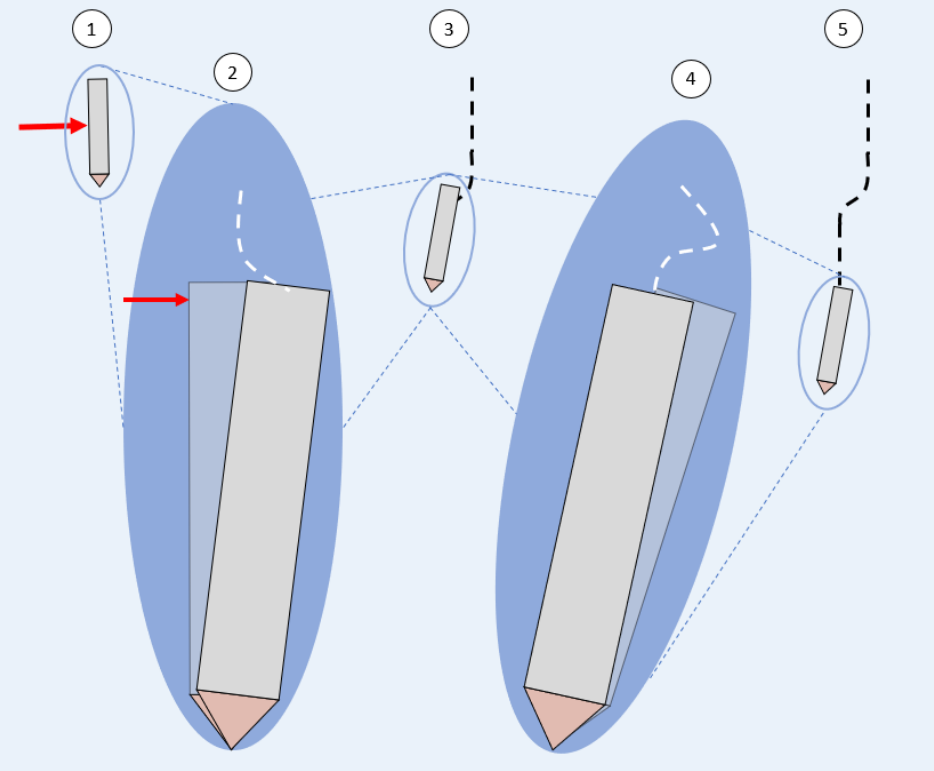

Fig. 19 Separation of dynamics. In this case, the melting dynamics depend on the orientation of the probe within the melt pocket only up to a certain pitch angle. The probe attains a sort of trim state (again, analogous to what might be observed for a launch vehicle) which increases the resistance to descent but does not cause instability or excessive off-vertical motion.

Then the criterion for static stability becomes

$$m|x_{CG}| < \rho_{wat}V|x_{CB}| \Rightarrow \rho_{probe}|x_{CG}| < \rho_{wat}|x_{CB}| \tag{22}$$

If the buoyant force and weight of the melt probe are equal – undesirable, since melting depends on the presence of downward force ensuring good contact between the ice and the melt head [26, 34] – then this condition becomes the general conditions for total stability of a submerged, floating object:

$$m = \rho_{wat}V \tag{23}$$

$$|x_{CG}| < |x_{CB}| \tag{24}$$

1. Comparison of Melt Probe Design

The condition on the center of mass as a fraction, f_{CG}, of the probe length in order to satisfy eq. (22) is given in the Table 8 for a number of ice-penetrating probe designs. In accordance with AP, x_{CB} is assumed to lie at each probe's center of volume.

Table 8 Melt Probe Buoyant Stability Criterion

Probe	L (m)	V (m^3)	m (kg)	ρ_{probe} (kg/m^3)	f_{CG} (x_{CG}/L)	Reference
Cryobot	1.25	0.0141	40	2840	< 0.176	[26]
IceMole 3	1.94	0.0437	60	1370	< 0.363	[25]
Tunnelbot (Reactor)	5.3	1.04	1350	1300	< 0.415	[13]
Tunnelbot (GPHS)	5.75	0.282	750	2660	< 0.189	[13]
VERNE	4.5	0.457	480	1050	< 0.475	[5]
SLUSH	3.00	0.0462	–	–	$< 23/m$	[14]
RECAS	4	0.0616	–	–	$< 30.7/m$	[19]
VALKYRIE	2.5	0.127	–	–	$< 63.2/m$	[15]
IceShuttle Toredo	6.9	0.425	–	–	$< 212/m$	[34]
SPINDLE	8	1.01	–	–	$< 504/m$	[15]

For probes with a low f_{CG} – directly correlated with a high average density – it is more constraining on the design to achieve buoyant stability. However, designs with a high f_{CG} – correlated with a low average density – have worse payload-to-power ratios, since any increase in volume (via an increase in length or radius) results in an increase in the required thermal power. In other words, although this may seem like a like simple requirement to impose on a melt probe design, it is not always judged to be worthwhile (for example, in [4]).

2. Applicability of Archimedes Principle

AP defines the buoyant force on an object as the weight of the liquid it displaces; however, it is actually a result of the total of all pressure forces exerted on an object by the fluid. AP gives identical results to this surface integral in its typical application: a body surrounded by an unbounded fluid of homogeneous density. However, scenarios can be constructed in which these results are not identical. For example, in [39, 40], it is shown that AP is not valid when an object submerged in a fluid makes a vacuum-sealed contact with the walls or floor of its container. Instead, the net pressure force includes a component pressing the object against said wall, and in the case of an object on the bottom of the container the conventional buoyant force is completely eliminated. Therefore, the question is posed: In the case of a melt probe, does AP still give the pressure force vector, $\vec{F}_p$?

A typical assumption in the field of close contact melting is that a thin film of fluid is always present between the heated element and the phase change medium [21, 34], precluding the exact exception described in [39, 40]. However, it should also be noted that the melt pocket is nonuniformly heated and fluid is continuously generated or removed at the phase boundaries, creating pressure and flow fields. It's possible that these pressure gradients exceed the gravitational pressure gradient that is responsible for the buoyant force, especially on a planetoid with lower gravity such as Europa.

Finding these pressure fields requires a solution of the partial differential equations of conservation of fluid mass, momentum, and energy. A 2-dimensional gridded solution of this problem for the film directly below a rectangular probe with a flat melt head is given in [34], and a 3-dimensional solution is provided in [24]. The iterative solution procedures developed in these papers have been replicated in the course of this project, but with little success due to convergence issues. Given this experience, it is believed that the modeling effort to generate a single purpose solution for the pressure field surrounding a 3-dimensional probe of arbitrary shape would be quite large. A more efficient method might be to apply a multiphysics tool such as StarCCM+ to perform CFD and/or FEA on the melting processes as done in [27], with the focus on the attitude stability rather than the rate of melting.

VI. Future Work

The ongoing task with the highest potential to increase the fidelity of the hybrid simulation is the development of a physics-based mechanical drilling model which covers the required solver ranges or has good extrapolation properties. Such a model is currently under investigation by several researchers on the VERNE project, and although no radically

different solution has yet been proposed, it may be possible to augment the current model with additional data points. Similarly, efficiency correction factors for the thermal power requirements could benefit from the collection of more field test data points of thermal probes, particularly at lower ice temperatures. A more in depth, test-informed analysis of the correct way to interpret a thermomechanical drill and the individual thermal and mechanical velocity contributions could also aid in selection between some of the different assumptions detailed in this paper.

A less straightforward but more accessible way to improve the trajectory simulations is to increase the convergence robustness. This approach will involve attempts to guarantee uniqueness and convergence of the discussed iterative procedures as well as experimenting with different initial conditions, residual weights, step sizes, and dynamic integrators.

Significant work may also be done on the problem of trajectory optimization. Useful optimization objectives include minimizing probe power and descent time, maximizing the portion of the ice shell where liquid samples can be taken, and optimizing the mechanical and thermal fluid loop design. Formulating and solving this problem as an optimal control problem could also provide more detailed results which could be easily reinterpreted given updated models of Europa's ice shell from future studies.

Finally, a sufficient dynamic model has yet to be developed to predict the pitch stability of a melt probe. Due to the complex relationships between the heating of the melt pocket, melt dynamics, and pressure forces on the probe, it is not clear whether there is a simple, closed-form modeling technique that will serve this purpose. The most promising path forward is expected to involve analysis with a multiphysics tool in order to develop a deck of stability derivatives which may be interpolated on, similar to those sometimes used for aircraft.

VII. Acknowledgements

This research was funded by the NASA SESAME program. Acknowledgements also go to research advisor Dr. Glenn Lightsey, project PI Dr. Britney Schmidt, and co-researchers Chase Chivers and Yashvardian Chandramouli.

References

[1] Bryson, F. E., Nassif, M., Szot, P. A., Chivers, C. J., Daniel, N., Wiley, B. E., Plattner, T., Hanna, A., Tomar, Y., Rapoport, S., Spiers, E. M., Pierson, S., Hodges, A., Dichek, D., Hughson, K., Meister, M. R., Lightsey, E. G., and Schmidt, B., "Vertical Entry Robot for Navigating Europa (VERNE) Mission and System Design," *ASCEND 2020*, American Institute of Aeronautics and Astronautics, ???? https://doi.org/10.2514/6.2020-4061, URL https://arc.aiaa.org/doi/abs/10.2514/6.2020-4061, _eprint: https://arc.aiaa.org/doi/pdf/10.2514/6.2020-4061.

[2] Aamot, H. W. C., "The Philberth Probe for Investigating Polar Ice Caps," *Cold Regions Research & Engineering Laboratory*, 1967.

[3] Aamot, H. W. C., "Heat Transfer and Performance Analysis of a Thermal Probe for Glaciers," *Cold Regions Research & Engineering Laboratory*, 1967.

[4] Tueg, H., and Damm, M., "Computer-controlled melting probe for detecting different measurement parameters in an area of ice has a melting head, a vertical control tube and sensors with very small recording areas for obtaining good local definition," , Feb. 2003. URL https://patents.google.com/patent/DE10164648C1/en.

[5] Alemany, O., Chappellaz, J., Triest, J., Calzas, M., Cattani, O., Chemin, J. F., Desbois, Q., Desbois, T., Duphil, R., Falourd, S., Grilli, R., Guillerme, C., Kerstel, E., Laurent, B., Lefebvre, E., Marrocco, N., Pascual, O., Piard, L., Possenti, P., Romanini, D., Thiebaut, V., and Yamani, R., "The SUBGLACIOR drilling probe: concept and design," *Annals of Glaciology*, Vol. 55, No. 68, 2014, pp. 233–242. https://doi.org/10.3189/2014AoG68A026, URL https://www.cambridge.org/core/journals/annals-of-glaciology/article/subglacior-drilling-probe-concept-and-design/D1A962F743FA39C0CD80200C0118FE3A, publisher: Cambridge University Press.

[6] Dachwald, B., Mikucki, J., Tulaczyk, S., Digel, I., Espe, C., Feldmann, M., Francke, G., Kowalski, J., and Xu, C., "IceMole: a maneuverable probe for clean in situ analysis and sampling of subsurface ice and subglacial aquatic ecosystems," *Annals of Glaciology*, Vol. 55, No. 65, 2014, pp. 14–22. https://doi.org/10.3189/2014AoG65A004, URL https://www.cambridge.org/core/journals/annals-of-glaciology/article/icemole-a-maneuverable-probe-for-clean-in-situ-analysis-and-sampling-of-subsurface-ice-and-subglacial-aquatic-ecosystems/A5174FD249A0CB4E8DFBE7B1935E1765, publisher: Cambridge University Press.

[7] Billings, S. E., and Kattenhorn, S. A., "The great thickness debate: Ice shell thickness models for Europa and comparisons with estimates based on flexure at ridges," *Icarus*, Vol. 177, No. 2, 2005, pp. 397–412. https://doi.org/10.1016/j.icarus.2005.03.013, URL http://www.sciencedirect.com/science/article/pii/S0019103505001211.

[8] Pappalardo, R., Head, J., Greeley, R., Sullivan, R., Pilcher, C., Moore, W., Carr, M., Moore, J., Belton, M., and Goldsby, D., "Geological evidence for solid-state convection in Europa's ice shell," *Nature*, Vol. 391, 1998, pp. 365–8. https://doi.org/10.1038/34862.

[9] McKinnon, W. B., "Convective instability in Europa's floating ice shell," *Geophysical Research Letters*, Vol. 26, No. 7, 1999, pp. 951–954. https://doi.org/https://doi.org/10.1029/1999GL900125, URL https://agupubs.onlinelibrary.wiley.com/doi/abs/10.1029/1999GL900125, _eprint: https://agupubs.onlinelibrary.wiley.com/doi/pdf/10.1029/1999GL900125.

[10] Nimmo, F., and Manga, M., "Geodynamics of Europa's Icy Shell," *Europa*, 2009.

[11] Zolotov, M., and Shock, E., "Composition and stability of salts on the surface of Europa and their oceanic origin," *Journal of Geophysical Research*, Vol. 106, 2001. https://doi.org/10.1029/2000JE001413.

[12] Buffo, J., Schmidt, B. E., Huber, C., and Walker, C. C., "Entrainment and Dynamics of Ocean-derived Impurities within Europa's Ice Shell," , Sep. 2020. https://doi.org/10.1002/essoar.10502079.3, URL http://www.essoar.org/doi/10.1002/essoar.10502079.3, archive Location: world Publisher: Earth and Space Science Open Archive Section: Planetology.

[13] Treffer, M., Kömle, N. I., Kargl, G., Kaufmann, E., Ulamec, S., Biele, J., Ivanov, A., and Funke, O., "Preliminary studies concerning subsurface probes for the exploration of icy planetary bodies," *Planetary and Space Science*, Vol. 54, No. 6, 2006, pp. 621–634. https://doi.org/10.1016/j.pss.2006.02.001, URL http://www.sciencedirect.com/science/article/pii/S0032063306000316.

[14] Kaufmann, E., Kargl, G., Kömle, N. I., Steller, M., Hasiba, J., Tatschl, F., Ulamec, S., Biele, J., Engelhardt, M., and Romstedt, J., "Melting and Sublimation of Planetary Ices Under Low Pressure Conditions: Laboratory Experiments with a Melting Probe Prototype," *Earth, Moon, and Planets*, Vol. 105, No. 1, 2009, pp. 11–29. https://doi.org/10.1007/s11038-009-9296-9, URL https://doi.org/10.1007/s11038-009-9296-9.

[15] Kömle, N. I., Tiefenbacher, P., and Kahr, A., "Melting probe experiments under Mars surface conditions – the influence of dust layers, CO2-ice and porosity," *Icarus*, Vol. 315, 2018, pp. 7–19. https://doi.org/10.1016/j.icarus.2018.06.012, URL http://www.sciencedirect.com/science/article/pii/S0019103518301088.

[16] Barr, A. C., and Showman, A. P., "Heat Transfer in Europa's Icy Shell," ????, p. 26.

[17] Oleson, S., Newman, J. M., Dombard, A., and Meyer-Dombard, D., "Compass Final Report: Europa Tunnelbot," 2019, p. 70.

[18] Zacny, K., Robotics, H., Mueller, J., Costa, T., Robotics, H., Cwik, T., Gray, A., Zimmerman, W., Chow, P., Robotics, H., Rehnmark, F., Robotics, H., and Adams, G., "SLUSH: Europa hybrid deep drill," *2018 IEEE Aerospace Conference*, 2018, pp. 1–14. https://doi.org/10.1109/AERO.2018.8396596.

[19] Stone, W., Hogan, B., Siegel, V., Harman, J., Flesher, C., Clark, E., Pradhan, O., Gasiewski, A., Howe, S., and Howe, T., "Project VALKYRIE: Laser-Powered Cryobots and Other Methods for Penetrating Deep Ice on Ocean Worlds," *Outer Solar System: Prospective Energy and Material Resources*, edited by V. Badescu and K. Zacny, Springer International Publishing, Cham, 2018, pp. 47–165. https://doi.org/10.1007/978-3-319-73845-1_4, URL https://doi.org/10.1007/978-3-319-73845-1_4.

[20] Weiss, P., Yung, K. L., Ng, T. C., Kömle, N., Kargl, G., and Kaufmann, E., "Study of a thermal drill head for the exploration of subsurface planetary ice layers," *Planetary and Space Science*, Vol. 56, No. 9, 2008, pp. 1280–1292. https://doi.org/10.1016/j.pss.2008.04.004, URL http://www.sciencedirect.com/science/article/pii/S0032063308000962.

[21] Shreve, R. L., "Theory of Performance of Isothermal Solid-Nose Hotpoints Boring in Temperate Ice*," *Journal of Glaciology*, Vol. 4, No. 32, 1962, pp. 151–160. https://doi.org/10.3189/S0022143000027362, URL https://www.cambridge.org/core/journals/journal-of-glaciology/article/theory-of-performance-of-isothermal-solidnose-hotpoints-boring-in-temperate-ice/964C1BDD51450D8D04157D36FD95C7AC/core-reader, publisher: Cambridge University Press.

[22] Ulamec, S., Biele, J., Funke, O., and Engelhardt, M., "Access to glacial and subglacial environments in the Solar System by melting probe technology," *Reviews in Environmental Science and Bio/Technology*, Vol. 6, No. 1, 2007, pp. 71–94. https://doi.org/10.1007/s11157-006-9108-x, URL https://doi.org/10.1007/s11157-006-9108-x.

[23] Talalay, P. G., Zagorodnov, V. S., Markov, A. N., Sysoev, M. A., and Hong, J., "Recoverable autonomous sonde (RECAS) for environmental exploration of Antarctic subglacial lakes: general concept," *Annals of Glaciology*, Vol. 55, No. 65, 2014, pp. 23–30. https://doi.org/10.3189/2014AoG65A003, URL https://www.cambridge.org/core/journals/annals-of-glaciology/article/recoverable-autonomous-sonde-recas-for-environmental-exploration-of-antarctic-subglacial-lakes-general-concept/9C2AC87D4E79CB6F27A217E9B6904696, publisher: Cambridge University Press.

[24] Schüller, K., and Kowalski, J., "Spatially varying heat flux driven close-contact melting – A Lagrangian approach," *International Journal of Heat and Mass Transfer*, Vol. 115, 2017, pp. 1276–1287. https://doi.org/10.1016/j.ijheatmasstransfer.2017.08.092, URL http://www.sciencedirect.com/science/article/pii/S0017931017317349.

[25] Schüller, K., and Kowalski, J., "Melting probe technology for subsurface exploration of extraterrestrial ice – Critical refreezing length and the role of gravity," *Icarus*, Vol. 317, 2019, pp. 1–9. https://doi.org/10.1016/j.icarus.2018.05.022, URL http://www.sciencedirect.com/science/article/pii/S0019103518301568.

[26] Li, Y., Talalay, P. G., Sysoev, M. A., Zagorodnov, V. S., Li, X., and Fan, X., "Thermal Heads for Melt Drilling to Subglacial Lakes: Design and Testing," *Astrobiology*, Vol. 20, No. 1, 2020, pp. 142–156. https://doi.org/10.1089/ast.2019.2103, URL https://www.liebertpub.com/doi/abs/10.1089/ast.2019.2103, publisher: Mary Ann Liebert, Inc., publishers.

[27] Brandt, M., Zimmerman, W., Berisford, D., Mueller, J., Barry, M., Durka, M., Kristof, R., Hogan, B., and Stone, W., "Modeling of Cryobot Melting Rates in Cryogenic Ice," *2019 IEEE Aerospace Conference*, 2019, pp. 1–17. https://doi.org/10.1109/AERO.2019.8741396, iSSN: 1095-323X.

[28] Poirier, D. R., and Geiger, G. H., "Conduction of Heat in Solids," *Transport Phenomena in Materials Processing*, edited by D. R. Poirier and G. H. Geiger, Springer International Publishing, Cham, 2016, pp. 281–327. https://doi.org/10.1007/978-3-319-48090-9_9, URL https://doi.org/10.1007/978-3-319-48090-9_9.

[29] Weinberg, K., and Ortiz, M., "Ice Penetration by a Bluff-Body Melting Probe," *Journal of Applied Mechanics*, Vol. 87, No. 6, 2020. https://doi.org/10.1115/1.4046633, URL https://asmedigitalcollection.asme.org/appliedmechanics/article/87/6/061003/1080843/Ice-Penetration-by-a-Bluff-Body-Melting-Probe, publisher: American Society of Mechanical Engineers Digital Collection.

[30] Kowalski, J., Linder, P., Zierke, S., von Wulfen, B., Clemens, J., Hoffmann, R., Mikucki, J., Tulaczyk, S., Funke, O., Blandfort, D., Espe, C., Feldmann, M., Francke, G., Hiecker, S., Plescher, E., Schöngarth, S., Schüller, K., Dachwald, B., Digel, I., Artmann, G., Eliseev, D., Heinen, D., Scholz, F., Wiebusch, C., Macht, S., Bestmann, U., Reineking, T., Zetzsche, C., Schill, K., Förstner, R., Niedermeier, H., Szumski, A., Eissfeller, B., Naumann, U., and Helbing, K., "Navigation technology for exploration of glacier ice with maneuverable melting probes," *Cold Regions Science and Technology*, Vol. 123, 2016, pp. 53–70. https://doi.org/10.1016/j.coldregions.2015.11.006, URL http://www.sciencedirect.com/science/article/pii/S0165232X15002852.

[31] Zimmerman, W., Bonitz, R., and Feldman, J., "Cryobot: an ice penetrating robotic vehicle for Mars and Europa," *2001 IEEE Aerospace Conference Proceedings (Cat. No.01TH8542)*, Vol. 1, 2001, pp. 1/311–1/323 vol.1. https://doi.org/10.1109/AERO.2001.931722.

[32] Garry, J., and Wright, I., "The Cutting Strength of Cryogenic Water Ice," 2000.

[33] Garry, J., and Wright, I., "Coring experiments with cryogenic water and carbon dioxide ices - Toward planetary surface operations," *Planetary and Space Science*, Vol. 52, 2004, pp. 823–831. https://doi.org/10.1016/j.pss.2004.03.003.

[34] Schüller, K., Kowalski, J., and Råback, P., "Curvilinear melting – A preliminary experimental and numerical study," *International Journal of Heat and Mass Transfer*, Vol. 92, 2016, pp. 884–892. https://doi.org/10.1016/j.ijheatmasstransfer.2015.09.046, URL http://www.sciencedirect.com/science/article/pii/S0017931015303653.

[35] Aamot, H. W. C., "Instruments and Methods: A Buoyancy-Stabilized Hot-Point Drill for Glacier Studies," *Journal of Glaciology*, Vol. 7, No. 51, 1968, pp. 493–498. https://doi.org/10.3189/S0022143000020670,

URL https://www.cambridge.org/core/journals/journal-of-glaciology/article/instruments-and-methods-a-buoyancystabilized-hotpoint-drill-for-glacier-studies/167F6902B88F09ED3C377AC362B79023, publisher: Cambridge University Press.

[36] Aamot, H. W. C., "Pendulum Steering for Thermal Probes in Glaciers," *Journal of Glaciology*, Vol. 6, No. 48, 1967, pp. 935–938. https://doi.org/10.3189/S0022143000020220, URL https://www.cambridge.org/core/journals/journal-of-glaciology/article/pendulum-steering-for-thermal-probes-in-glaciers/291F7719D7B745299E51C9458818561A, publisher: Cambridge University Press.

[37] Allen, D. W., Jones, M., McCue-Weil, L. S., Woolsey, C. A., and Moore, W. B., "Exploration of under-ice regions with ocean profiling agents (EUROPA)," Report, Virginia Center for Autonomous Systems, Sep. 2013. URL https://vtechworks.lib.vt.edu/handle/10919/82061, accepted: 2018-02-12T15:34:24Z.

[38] Wirtz, M., and Hildebrandt, M., "IceShuttle Teredo: An Ice-Penetrating Robotic System to Transport an Exploration AUV into the Ocean of Jupiter's Moon Europa," 2016.

[39] Lima, F. M. S., "Using surface integrals for checking the Archimedes' law of buoyancy," *European Journal of Physics*, Vol. 33, No. 1, 2012, pp. 101–113. https://doi.org/10.1088/0143-0807/33/1/009, URL http://arxiv.org/abs/1110.5264, arXiv: 1110.5264.

[40] Bierman, J., and Kincanon, E., "Reconsidering Archimedes' Principle," *The Physics Teacher*, Vol. 41, 2003, pp. 340–344. https://doi.org/10.1119/1.1607804.